FULL PAPER

ADVANCED FUNCTIONAL MATERIALS

DOI: 10.1002/adfm.200700673

Hierarchical Assembly of Organic/Inorganic Building Molecules with π–π Interactions**

By *Lu Yang, Huisheng Peng, Kun Huang, Joel T. Mague, Hexing Li,** and *Yunfeng Lu**

Hierarchical assemblies of perylenetetracarboxylic diimide bridged silsesquioxane (PDBS) with controlled structure at multi-length scale are studied using both experimental and computational methods. The organization process spans multi-length scales and includes three continuous steps: 1) stacking of the preprogrammed molecules into small clusters, 2) growing of the small clusters into nanoscale building blocks with various sizes and shapes depending on the experimental conditions, and 3) aggregation of nanoscale building blocks into micro- or macro-scale assemblies. The main factors determining the assembly morphology are the second and third steps, which can be controlled by varying the experimental conditions, such as solution drying rate, solvent composition, and PDBS concentration. Despite the different morphologies, all of these assemblies possess highly ordered lamellar structure. It is found that incorporating perylenetetracarboxylic diimide (PD) moieties into the highly ordered silica network endows the PD components with high thermal and mechanical stability, as well as improved optical and electronic properties.

1. Introduction

Inspired by nature's ability to create extraordinarily well-defined objects from simple components, researchers have been attempting to synthesize materials with predetermined structure and composition from relatively simple molecules.[1] Self-assembly, the directed organization of molecular building blocks over multiple length scales, is widely used for the synthesis of such materials. During assembly, molecular building blocks carrying key information of structure, composition, and function are organized into well-defined structures driven by noncovalent interactions, such as hydrogen bonding, π–π stacking, electrostatic interactions, and hydrophobic interactions.[2–8] To date, numerous interesting materials have been assembled from a large library of molecular building blocks, including inorganic complex and clusters,[9] dendrite molecules with controlled shapes,[10] amphiphilic molecules with controlled hydrophilic/hydrophobic interactions,[11] organic oligomers that form hydrogen bonding networks,[12] and hybrid organic/inorganic molecules or clusters.[13]

Hierarchical assembly from nano-, micro-, meso- to macro-scales is of particular importance. Through design and synthesis of the molecular building blocks, novel self-assembled materials with hierarchically controlled structure, precisely defined composition as well as unique electronic, magnetic, and optical properties can be obtained in a cost effective and timely manner. Recent advances in the syntheses of polypeptide fibers,[3a] polymer macroscopic tubes,[8b] and hybrid micro-tubes[5] from chiral polypeptide, block copolymer and organic/inorganic building blocks, respectively, shield light on this endeavor. How these building blocks assemble into these microscopic and/or macroscopic assemblies, however, remains to be elucidated.

This work reports the hierarchical assembly of perylenetetracarboxylic diimide bridged silsesquioxane (PDBS) that forms micro- or macro-spheres, tubes and fibers. The reasons for choosing PDBS as our model building block are potential applications of perylenetetracarboxylic diimide (PD) derivatives in

[*] Prof. H. Li
Department of Chemistry, Shanghai Normal University
Shanghai 200234 (P. R. China)
E-mail: hexing-li@shnu.edu.cn
Prof. Y. Lu
Department of Chemical and Biomolecular Engineering, University of California
Los Angeles, CA 90095 (USA)
E-mail: luucla@ucla.edu
Dr. L. Yang
Theoretical Chemistry & Molecular Physics (T-12) Group, Los Alamos National Laboratory
Los Alamos, NM 87545 (USA)
Dr. H. Peng, Dr. K. Huang
Department of Chemical and Biomolecular Engineering,
Tulane University
New Orleans, Louisiana 70118 (USA)
Prof. J. T. Mague
Department of Chemistry, Tulane University
New Orleans, Louisiana 70118 (USA)

[**] Dr. Lu Yang and Dr. Huisheng Peng contributed equally to this work. This work was partially supported by ONR, NSF-CARRER Award, and Sandia National Laboratories. The authors thank Dr. Jibao He for the TEM characterization, Dr. Weilie Zhou for the SEM characterization, Dr. Louise Braud Nohyphen and Dr. Kyriakos D. Papadopoulos for the optical and fluorescent microscopic measurement, and Dr. Jiebin Pang for useful discussion. Los Alamos National Laboratory is operated by Los Alamos National Security, LLC, for the National Security Administration of the U. S. Department of Energy under contract DE-AC52-06NA25396. Supporting Information is available online from Wiley InterScience or from the authors.

ADVANCED FUNCTIONAL MATERIALS

optical signal processing, electrophotography, and solar energy conversion, etc.[14–18] In addition, bridged silsesquioxane represents a class of organic/inorganic building molecules with a molecular structure of $(RO)_3$–Si–R′–Si–$(RO)_3$, where OR is a hydrolysable alkoxide group (e.g., CH_3O– and CH_3CH_2O–) and R′ is a non-hydrolysable functional group, such as phenyl, octyl, aminoalkyl, cyanoalkyl, thioloalkyl, epoxyl, vinyl and conjugated diacetylenic groups.[19–29] Tuning noncovalent interactions among these building molecules (e.g., π–π interactions among the conjugated bridging organic moieties) allows precise control over the assembling structure. Furthermore, hydrolysis and condensation reactions of the alkoxysilane substituents create inorganic silica framework that is covalently bonded with organic moieties, resulting in organic/inorganic nanocomposites with unique or greatly enhanced properties. Utilizing both experimental and computational techniques, we probed the assembly process of PDBS at multi-length scales and proposed a pathway of hierarchical assembly. This work not only provides an efficient approach toward the design and synthesis of novel hybrid nanocomposites with enhanced properties, the insights gained from the hierarchical assembly is also useful for designing novel intelligent materials.

2. Results and Discussion

2.1. PDBS Assemblies with Tunable Morphologies

Figure 1 shows fluorescent optical micrograph (a), optical micrograph (b), transmission electron microscope (TEM) image (c), and X-ray diffraction (XRD) (d) of the assembled PDBS micro-tubes, prepared by casting PDBS THF/petroleum ether solution (initial concentration of 8.3 mg mL^{-1}) on glass substrates at room temperature (air drying for ~5 minutes). As shown from Figure 1a and b, these micro-tubes have outside diameters (OD) of 5–10 micrometers, inside diameter (ID) of 3.5–7 μm and length up to millimeters. The TEM image clearly reveals a highly ordered lamellar structure with an interlamellar distance of ~2.7 nm, consistent with the length of the molecular building block calculated from Molecular Mechanical Geometry Optimization (2.9 nm). The XRD result of these tubes shows intense Bragg (00*l*) peaks indicating a long-range lamellar structure with a *d*-spacing 2.7 nm, in good agreement with the TEM observation.

The morphology of the PDBS assemblies dramatically changes with different assembly conditions. For example, casting the same PDBS solution on glass substrates at a higher temperature, e.g., 65 °C (air drying in ~10 seconds) and 90 °C (air drying in ~5 seconds), produced micro-fibers with reduced diameter and length (Fig. 2a and b). On the other hand, if we evaporate the solvent over a period of days at room temperature, macro-fibers with a diameter of 0.4 mm and length up to 1 cm are obtained (Fig. 2c and d). Interestingly, these macroscopic fibers are composed of micro-tubes (marked with an arrow) similar to those shown in Figure 1. The initial PDBS concentration also plays an important role in morphology. Casting a PDBS THF/petroleum solution with a lower PDBS concentration (2.7–3.3 mg mL^{-1}) on glass substrate at room temperature, for instance, produced hollow microspheres (air drying ~5 minutes). Figure 2e shows a typical fluorescent micrograph of the hollow spheres with an average diameter of 10.9 μm and a polydispersity of 0.1 estimated from one hundred cases. Solvent composition also affects the morphology. By adding water to the PDBS THF solution we rapidly precipitated solid spheres with an estimated diameter of 5.8 μm and a polydispersity of 0.05 (see the fluorescent microscopy in Fig. 2f). In addition, we noticed that substrates did not significantly affect the assembly behavior of PDBS molecules. Coating the PDBS solution on quartz and mica under similar conditions resulted in assemblies with morphologies similar to those on glasses (Fig. S2). Furthermore, similar XRD patterns are also observed for these morphologies, indicating their highly ordered lamellar structure at nanometer scale.

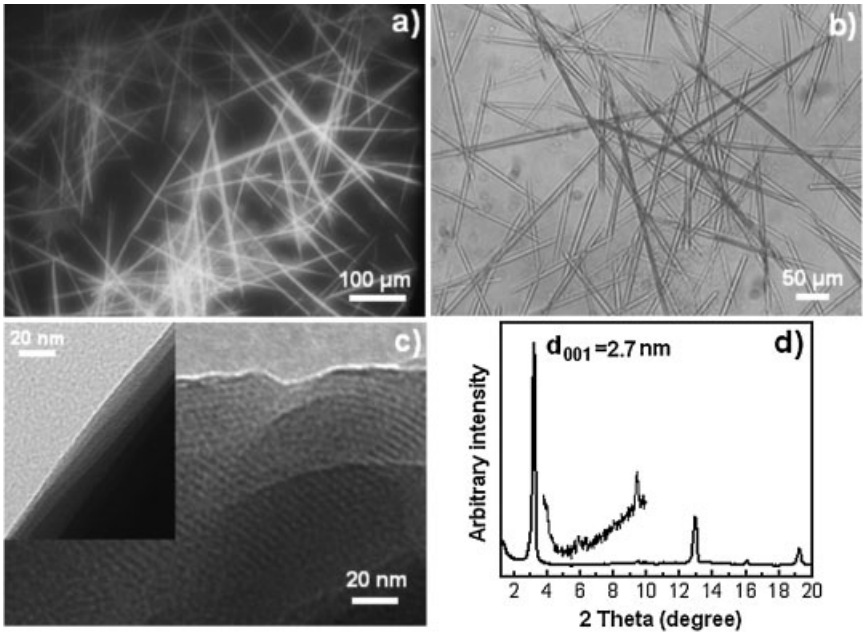

Figure 1. Micrometer-sized tubes prepared by coating PDBS THF/petroleum ether (v/v 1/5, concentration 8.3 mg mL^{-1}) solution on glass at room temperature. a) fluorescent micrograph; b) optical micrograph; c) TEM image; d) XRD patterns.

2.2. PDBS Assemblies with Unique Properties

As demonstrated above, PDBS self-organizes into hierarchical assemblies

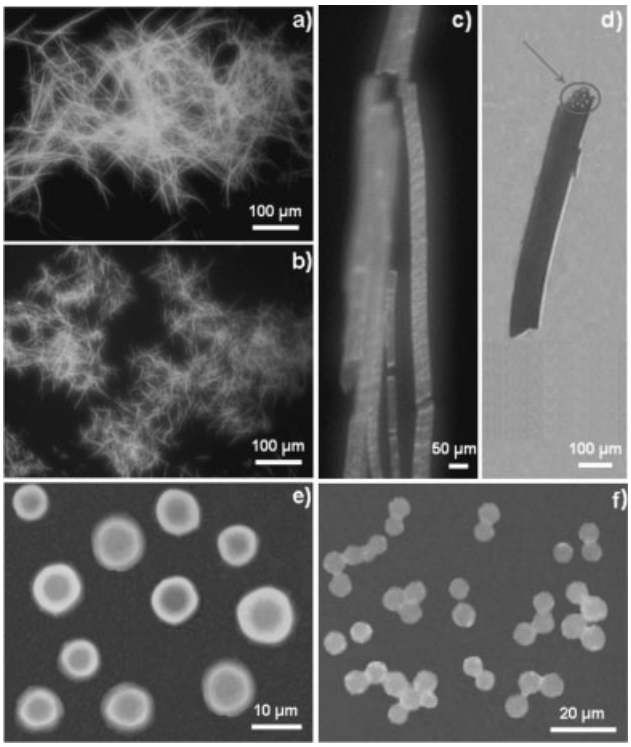

Figure 2. Fluorescent and optical micrographs of the hybrid PDBS aggregates with the other morphologies except micrometer-sized tubes (already shown in Fig. 1). a). Coating PDBS THF/petroleum ether (v/v 1/5, concentration 8.3 mg mL^{-1}) solution on the hot glass with a temperature of ~65 °C. b). Coating PDBS THF/petroleum ether (v/v 1/5, concentration 8.3 mg mL^{-1}) solution on the hot glass with a temperature of 90 °C. c) and d). Very slow evaporation (air drying ~ two weeks) of PDBS THF/petroleum ether (v/v 1/5, concentration 8.3 mg mL^{-1}) solution. e). Evaporation of PDBS THF/petroleum ether solution (v/v 1/5, concentration 2.7–3.3 mg mL^{-1}) at room temperature. f). Evaporation of PDBS THF/H_2O solution (v/v 1/5, concentration 2.7–3.3 mg mL^{-1}) at room temperature.

with ordered mesostructure and controlled morphology. Self-organization of these building molecules aligns the perylenetetracarboxylic diimide (PD) moieties, endowing these materials with unique properties. Figure 3 (left) shows the UV-vis spectra of PDBS solution as a function of evaporation time and the assembled tubes. The UV-vis spectrum of PDBS dilute solution shows three intense peaks at 454, 485, and 520 nm (bottom line), which were red shifted and formed a broad absorbance band upon the formation of PDBS tubes. Such red-shift phenomena have been reported in other assembled PD systems and have been attributed to the highly ordered molecular organization that allows more efficient π–π stacking and energy transport among the bridging PD moieties.[30–36] Figure 3 (right) shows the fluorescence spectra of PDBS solution and the assembled aggregates with different morphologies. Similarly, these aggregates show evidently red-shift as compared to PDBS spectrum in dilute solution. At the same time, the fluorescence intensity decreased, indicating the presence of strong fluorescence quenching effect with the formation of the aggregates. The large red shift and quenching in emission indicate strong intermolecular π–π stacking, which are associated with large exciton diffusion lengths[37–42] and high charge carrier mobility [43,44] Interestingly, the fluorescence spectra of hollow and solid micro-spheres show broader emission peak and larger red shift as compared to the spectrum of micro-tubes. Such an observation indicates that the fluorescence property is related to the assembly morphology, and a longer-range order resulted from a larger-length-scale assembly may provide more significant intermolecular interactions. The efficient π–π stacking provides the assemblies with enhanced electron conductivity. For example, the assembled tubes show an electron conductivity of 10^{-7} S cm^{-1} measured by the four-point contact method at room temperature, indicating that these PDBS tubes are semiconductive materials. This method provides a platform towards the synthesis of novel optoelectronic materials with the improved performance, due to the

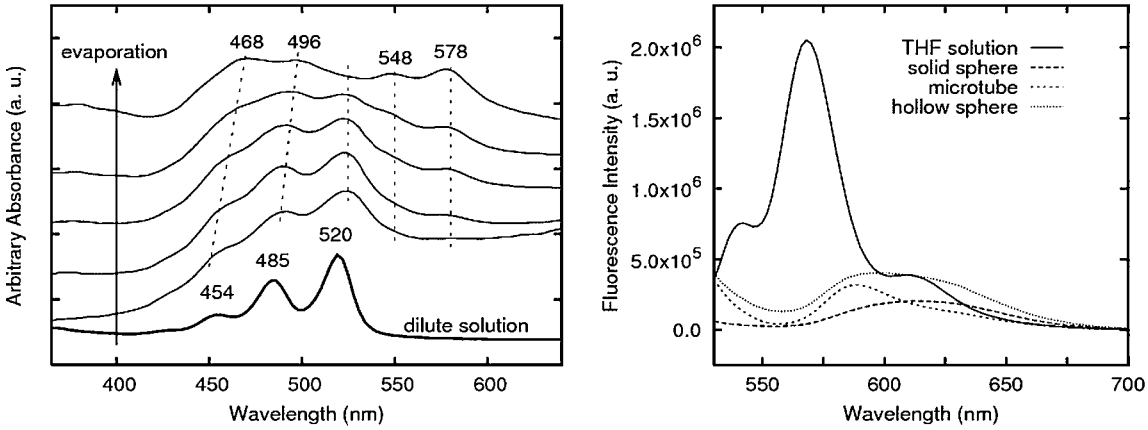

Figure 3. Left: Representative UV-vis spectra of PDBS THF/petroleum ether solution cased on quartz as a function of time. The arrow indicates time of evolving during UV-vis measurements. Dashed lines are added to guide the eye. Right: Fluorescence spectra of the PDBS THF solution and the asemblies with different morphologies.

ADVANCED FUNCTIONAL MATERIALS

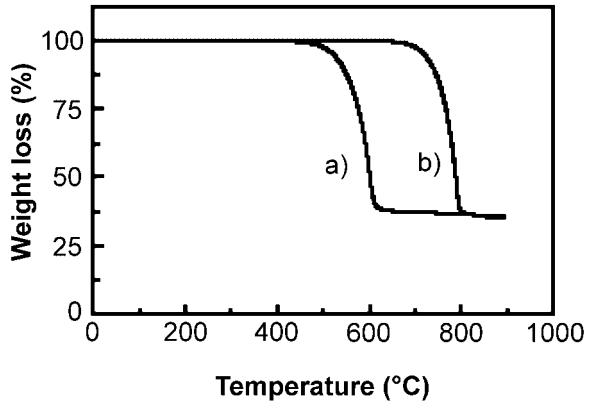

Figure 4. TGA thermographs of a) the precursor perylenetetracarboxylic diimide and b) PDBS tubes.

capability to align the bridging functional moieties through the simple assembly process.

Upon hydrolysis and condensation reactions of the alkoxysilane groups, inorganic silica framework were formed, resulting in organic/inorganic nanocomposites with greatly enhanced thermal stability. Figure 4 shows the thermogravimetric analysis (TGA) of the perylene and the tubular assemblies. The precursor undergoes decomposition at about 600 °C, while the PD/silica tubular nanocomposite loses their bulk weight at a much higher temperature (~800 °C), indicating a greatly improved thermal stability. Starting with perfectly tubular assemblies, no shape deformation was observed for the tubes even heated to a temperature of 950 °C for 2.5 hours in nitrogen (Fig. S3).

The highly ordered PDBS structure may also provide the assemblies with enhanced mechanical stability. By observing osmotically induced deformations, Möhwald et al. recently reported the mechanical stability of polymer/silica hybrid hollow spheres fabricated through a layer-by-layer absorption technology.[45] The rigid organic/inorganic structure is believed to be responsible for the deformation-resistant property of such systems, although the multilayer shell is in fact not highly ordered. The hybrid assemblies presented in this work are composed of highly ordered organic and silica layers, possibly providing the assemblies with higher mechanical stability.

3. Self-Assembly Mechanism Study

Each PDBS molecule can be considered as an amphiphilic building block relative to THF and petroleum ether, since it contains the propyltriethoxysilane moiety with good solubility and PD moiety with poor solubility in petroleum ether and THF. During casting, increasing the PDBS concentration promotes assembly. Figure 5 illustrates a possible assembling mechanism, which include the following steps: 1) the formation of nanoscale PDBS clusters through π–π interactions among neighboring PD moieties, 2) the growth of the clusters into various building blocks in which the propyltriethoxysilane moieties are maximally extended to solvent and the PD moieties are minimally contacted with solvent, and 3) the formation of micro- or macro-scale assemblies with different morphology from building blocks with controlled size and shape. Details of the proposed assembling mechanism are discussed below.

3.1. Self-Organization of PDBS into Molecular Clusters

Beginning with a homogenous PDBS solution, solvent evaporation during the casting process enriches PDBS molecules and promotes their association. While it is difficult to directly investigate the association *in situ*, UV-vis spectra of PDBS THF/petroleum ether solutions cast on quartz were collected as a function of time to illustrate the assembling of PDBS from free molecules to clusters and to micro-assemblies. As shown in Figure 3 (left), the UV-vis spectrum of the dilute PDBS solution shows three pronounced peaks in the range of 450–525 nm, which is consistent with previous studies on PD derivatives.[46] Upon casting on quartz, the THF and petroleum ether solvents evaporate from the substrate surface, resulting in a broadened absorption band, which is typically a sign of PDBS aggregation. The following successive UV-vis spectra clearly depict a red shift for about 12 nm. Such a spectral change implies strong π–π interactions among PD moieties. In addition, we observed two new peaks emerging around 548 nm and 578 nm. Both the red shift and the absorption band emerging at longer wavelength indicate the stacking of the PDBS molecular building blocks. This is also confirmed by the red shift and quenching in fluorescence emission.

Molecular simulations were also applied to probe details of the stacking/packing of PDBS in solvent. Ideally, the simulation of PDBS precursors in solution should be conducted to mimic the experiment. However, the molecular association process at present system is on the timescale of seconds, making rigorous molecular dynamics simulation study computationally prohibitive. It is well known that the primary driving force for the self-assembly of PD derivatives are the attractive π–π interactions between the perylene moieties, the strong dipolar interaction between the diimide moieties, and the van der Waals forces between alkyl chains.[47] To speed up the association process, silicon groups $Si(OEt)_3$ were removed from the ends, resulting in a *N*,*N*′-bispropyl-3,4,9,10-perylenetetracarboxylic diimide (BPD) molecule. We performed molecular dynamics simulations for BPD molecules in THF solution using AMBER 8.[48] The initial structure of the system was constructed by randomly putting 18 BPD molecules in a box of THF (374 molecules) with a minimum distance of 10 Å between the center of these BPD molecules (Fig. 6a). At the start of the simulation, the coordinates of the BPD molecules were constrained with an external harmonic potential and THF molecules were equilibrated for 200 picoseconds (ps). The BPD molecules were then released

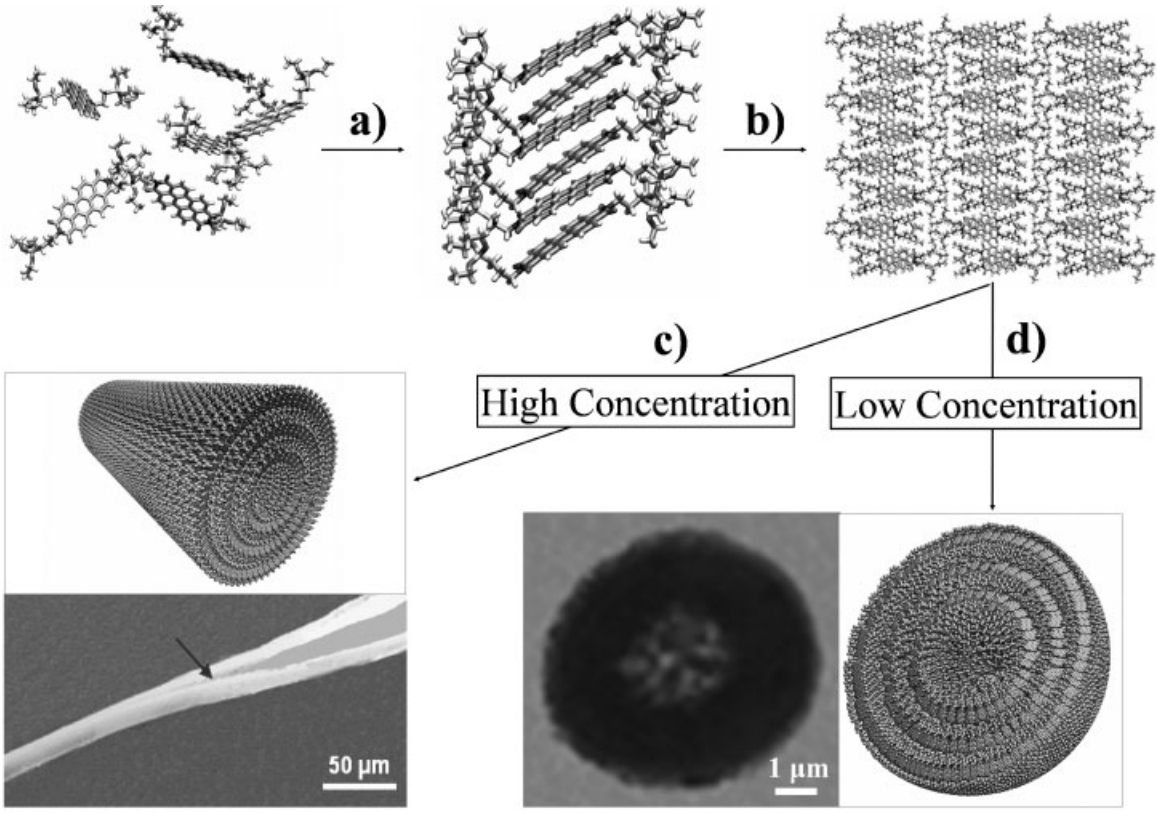

Figure 5. Schematic illustration of a) the proposed stacking of PDBS molecular building blocks, b) the aggregating of the proposed self-assembled clusters, c) the formation of macro-tubule (the bottom SEM picture shows the transition state of the tube formation) and d) the formation of hollow spheres (left, an optical micrograph).

and the simulation was extended for 5 nanoseconds (ns) to monitor the self-assembly process of BPD molecules.

The General AMBERR force field,[49] as implemented in the AMBER 8 package,[48] was used to describe the interactions of BPD and THF molecules in the system with the atom type and partial charge assigned by antechamber package. Periodic boundary conditions were applied and electrostatic interactions were calculated using the particle mesh Ewald (PME) method.[50] Hydrogen atoms were constrained at their ideal bond distance using the SHAKE algorithm.[51] Berendsen's coupling algorithms[52] were used to maintain constant temperature of 300 K and pressure of 1 atm. A time step of 2 femtoseconds was used in the simulation and coordinates were stored every picosecond for further analysis.

Figure 6a and b shows representative snapshots of the system before and after equilibration. When the constraints on the BPD molecules were removed, these randomly distributed molecules aggregate spontaneously and stacked together into highly ordered clusters in nanosecond time scale. During the aggregation process, BPD molecules first assemble into several stacks, followed by a slower process during which the resultant stacks float together, slowing further association into a single larger stack.

To obtain information about the orientation of BPD molecules in each stack, the radial distribution function for the center is calculated. As shown in Figure 6c, the maximum probabilities for the center-to-center distances between the BPD in solution were observed at 4.0 Å, 7.1 Å, and 10.7 Å. The sharp peak at 4.0 Å indicates that the structure of the BPD stack is considerably stable. The probability distribution function (PDF) for the face-to-face distances of the perylene moiety within the first shell was also calculated (Fig. 6c). The sharp peak at 3.5 Å, instead of 4 Å, suggests that the BPD molecule in each stack is shifted longitudinally with respect to the underlying molecule. This shift is to minimize the steric and electrostatic repulsion arising from the alkyl chains and the tetracarboxylic diimide moieties, respectively. In addition, we also calculated the probability distribution functions for the angles made by the perylene planes in the same stack (Fig. 6d). The nearly constant value of 1 for the $\cos(\theta)$, in which θ is the angle made by the normal vector of the planes, shows that the BPD molecules stack in a parallel fashion. Interestingly, the $\cos(\theta)$ for the angle between the long axis of the perylene planes showing a peak at 0.9, suggests that every perylene plane is rotated by approximately 25° with respect to the underlying molecules. Furthermore, the direction of the rotation for the perylene seems to be interlaced in the stack as indicated by the second peak at 1. This observation explains the previous results that the second and the third peak of the radial distribution function for the center of perylene moiety are

ADVANCED FUNCTIONAL MATERIALS

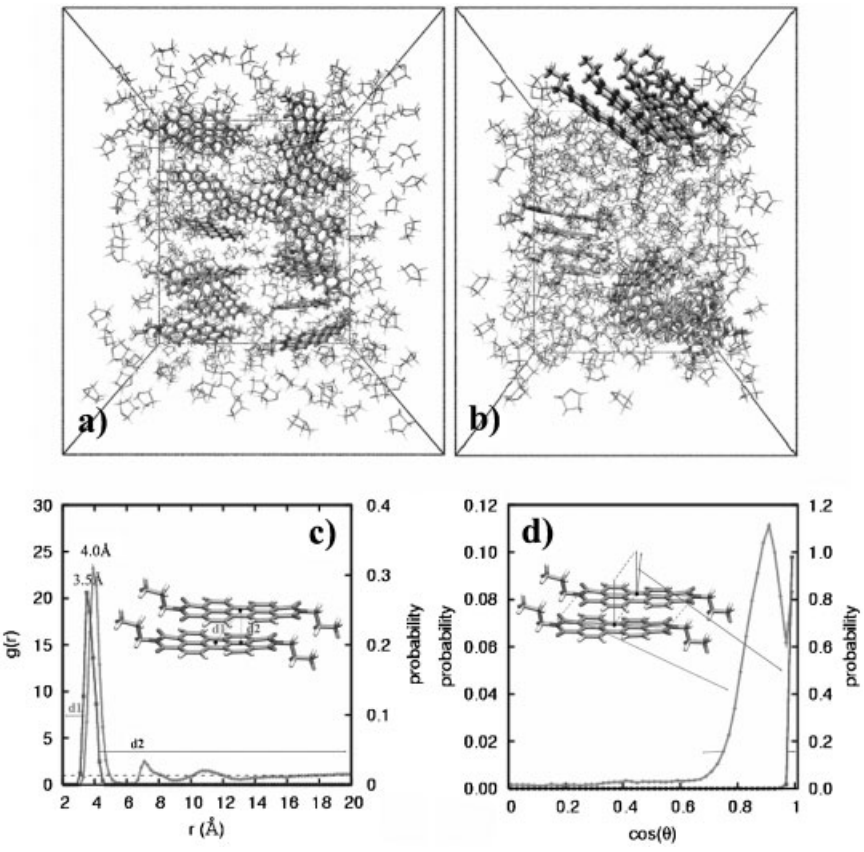

Figure 6. Self-assembly of *N,N′*-bispropyl-3,4,9,10-perylenetetracarboxylic diimide (BPD) in tetrahydrofuran (THF) solution. a). Representative snapshot of 3D simulation box before equilibrium. b). Representative snapshot of 3D simulation box equilibrated for 5 nanoseconds. The BPD is shown with thick sticks and the THF is shown with thin sticks. c). Radial distribution function, $g(r)$, for the center of PD unit (left *y* axis) and the probability distribution function for the planar distance between two neighboring PD (right *y* axis). d). Probability distribution function for the angle between the long axis of adjacent PD units (left coordinate) and the angle between the normal vector of adjacent PD planes (right *y* axis). Insert is the representative molecular structure of BPD obtained from Molecular Dynamic simulations.

located at 7.1 Å and 10.7 Å, instead of 8 Å and 12 Å, respectively. Based on these calculations, we can conclude that the BPD molecules stack parallel with longitudinal offset and transverse rotation between adjacent BPD moieties. This arrangement is driven by optimization of the steric repulsion, π–π stacking, and dipole–dipole interactions between the BPD molecules in different layers. Similar packing behavior has also been observed for other perylene derivatives.[28a,53]

In order to verify above simulation observation, we conducted single crystal X-ray diffraction of the PDBS micro-tubes, indicating a monoclinic crystal lattice with a $P2(1)/c$ space group. The unit cell parameters are $a = 28.56$ Å, $b = 17.58$ Å, $c = 8.09$ Å, $\alpha = 90°$, $\beta = 95.71°$, $\gamma = 90°$. Figure 7 shows the crystal structure of four PDBS precursors in a unit cell. The positioning of the two PDBS molecules in a stack exactly follows the same pattern as determined by molecular dynamics simulations, confirming that the MD simulation of BPD captured the key factors of PDBS assembly. The center-to-center distance between the adjacent PDBS precursors is ~4 Å while the face-to-face distance is ~3.5 Å, indicating the longitudinal offset of the neighboring molecules. As expected, the PD plane also rotated traversely around an axis perpendicular to the plane, which is well consistent with the molecular simulation results.

3.2. Growth and Organization of PDBS Molecular Clusters

The PDBS molecular stacks (as illustrated in Fig. 5b and c) grow into larger-dimension clusters with the evaporation of solvent. Depending on assembling conditions (e.g., PDBS concentration, solvent evaporation rate), building clusters with various dimensions and shapes will be formed. Such a cluster growth involves stacking of PDBS molecules in both face-to-face (perpendicular to the PD plane) and edge-by-edge (parallel to the PD plane) directions. From the molecular dynamics simulations we observed that the aggregation rate of BPD molecules in face-to-face direction is much faster than that of edge-by-edge direction due to the strong π–π stacking among the PD moieties. We therefore believe that the building clusters grown at favorable condition (e.g., high PDBS concentration and slow solvent-evaporation rate) may possess an elongated columelliform topology with the long axis perpendicular to the PD plane. The length and size of such clusters depend on the balance between the energy gain and the entropy loss of those PDBS molecules during the assembling process. For comparison, unfavorable growth conditions, such as low PDBS concentration and fast solvent-evaporation rate, may limit the cluster growth and generate smaller clusters with smaller aspect ratios (e.g., planar or cubic clusters), due to slower PDBS diffusion, depletion of PDBS source, or shorter growth period.

Assembly of such building clusters leads to the formation of microscopic or macroscopic assemblies with morphology governed by the cluster shape and size, as well as the assembling kinetics. At high PDBS concentration, the PDBS molecular stacks grow into columelliform clusters, which may directly assemble into tubes with the diameter and length of such tubes determined by the size of those building blocks. This mechanism explains the phenomena that small tubes are formed under high temperatures (fast drying rate) while large tubes are formed under low temperature (slow drying rate). In

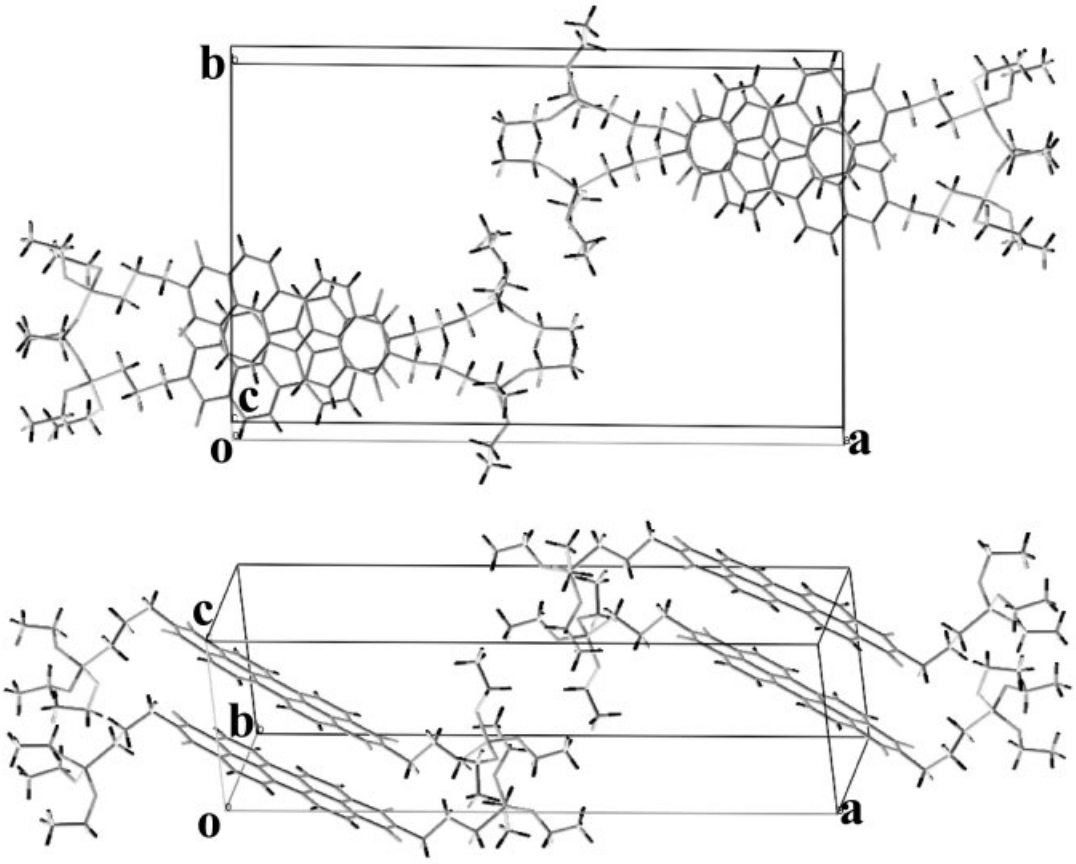

Figure 7. Crystal structure of the PDBS micro-tubes.

fact, if we remove the THF and petroleum ether solvent slow enough (e.g., drying the solvents in days), these resultant micro-tubes may further serve as building blocks and assemble together to form the macro-fibers as shown in Figure 2 c and d. For comparison, small planar or cubic clusters formed at low PDBS concentration may assemble together in favor of (hollow) spherical conformation to minimize the unfavorable interfacial energy between PDBS and the solvent, resulting in the formation of hollow PDBS spheres (see Fig. 5d). Note that all PDBS assemblies show highly ordered lamellar structure with the same *d*-spacing of 2.7 nm in spite of the different morphologies, further suggesting that the microscopic and macroscopic assemblies are indeed assembled from the building clusters.

Based on the experimental and simulation studies presented above, in particular, the fact that all PDBS assemblies with different morphologies show similar lamellar structure, we believe that the assembling mechanism of PDBS molecules at molecular level is similar. It is the difference in shape and size of the intermediate building blocks, which are controlled by various assembling conditions such as, the PDBS concentration, the solvent evaporation rate and the solvent compositions, leads to different morphologies of PDBS assemblies. In previous study,[46a] only small plates with lamellar structure were observed from evaporating PDBS-acetone (acetone is a good solvent as THF in this study) solution and they conclude that petroleum ether plays a specific role in the formation of PDBS tubes. However, we believe that the key factor for various morphologies is the kinetics of the aggregation process. For example, during our crystallization process, millimeter scale needles are also obtained with the slow vapor diffusion of diethyl ether into a concentrated THF/PDBS solution. Therefore, we argue that the role of petroleum ether in the tube formation process may only be reflected in its effect on the kinetics of assembly.

The hierarchical assembly scheme of PDBS can be generalized to other molecular assembling systems containing strong π–π interactions. As stated above, self-assembly process is generally driven by noncovalent interactions, such as Van der Waal interactions, hydrogen bonding, and π–π stacking. Generally, the strength of Van der Waal interactions is weaker than π–π stackings and hydrogen bonding. The construction of effective π–π interactions, however, requires precise alignment and stacking of the conjugated molecular moieties (e.g., the PD moiety) to enable maximum π-electron overlap. Such directional intermolecular interactions subsequently endow the building clusters with preferred growth directions, resulting in the formation of building clusters with specific topologies (e.g.,

ADVANCED FUNCTIONAL MATERIALS

elongated PDBS columns). Depended on assembling kinetics, the preferred growth may be promoted or retarded, generating intermediated building blocks with various shapes and sizes. Further assembling of these intermediated building blocks creates assemblies with tunable morphologies depend on the balance between the energy gain and the entropy loss during the assembling process. In the process of checking the applicability of this assembling scheme to other systems containing strong π–π interactions, we have also discovered that polyallylamine and long-chain conjugative acids can assemble into microscopic or macroscopic spheres and tubes depended on the assembly kinetics and molecular architecture. Detailed results will be published elsewhere. This hierarchical assembly mechanism has a significant implication for designing novel intelligent materials with controlled composition, structure, and morphology for a broad spectrum of applications. It may be also generalized to other molecular assembling systems with strong directional interactions.

4. Conclusions

Perylenetetracarboxylic diimide bridged silsesquioxane (PDBS) was synthesized and used to construct micro- and macro-assemblies through hierarchical assembly in solution. Optical, SEM, and fluorescent images indicate that the morphology of these assemblies is tunable from micro-tubes, macro-fibers, hollow spheres, to dense spheres. XRD and TEM results show that all assemblies possess similar ordered mesostructure. Molecular dynamic simulations combined with spectroscopic studies were used to investigate the assembling mechanism, which includes three major steps: 1) formation of molecular stacks from the free building molecules through balancing the steric repulsion, π–π stacking, and dipole–dipole interactions, 2) preferred growth of the molecular stacks into intermediated building blocks along the π–π interaction direction, and 3) organization of the intermediated building blocks into micro- or macro-assemblies depends on the balance between the energy gain and the entropy loss during the assembling processes. It was found that directional intermolecular interactions are the key to the structure and morphology of the assemblies. While assembling kinetics, which is dependent of experimental conditions such as drying rate of solvent, initial PDBS concentration and solvent composition, also significantly alters the assembling morphology. Such a precise hierarchical assembly of PDBS molecules endows the nanocomposites with improved thermal stability, unique optical property, enhanced electric conductivity, and superior mechanical stability, providing unique material platforms for optoelectronic and other device applications. Moreover, this multi-scale assembling scheme can be generalized to similar assembling systems containing strong directional intermolecular interactions, such as π–π interactions. The capability of organizing pre-designed building molecules into micro- or macro-scopic assemblies with controlled structure, composition and morphology is of great importance for novel material design and synthesis, as well as the construction of intelligent assembling systems.

5. Experimental

Synthesis of PDBS: (0.7 g (1.8 mmol)) of 3,4,9,10-perylenetetracaboxylic dianhydride and (1.9 ml (8 mmol)) (3-aminopropyl) triethoxysilane were added into a multi-neck flask. The flask was repeatedly evacuated and flushed with argon gas. The mixture was stirred for several minutes under argon atmosphere, then heated to ~120 °C in an oil bath. The reaction was held overnight. After cooled to room temperature, the product was washed with petroleum ether to remove the excess (3-aminopropyl) triethoxysilane. Scheme 1 shows the reaction and the chemical structure of the PDBS building blocks, which are stable in the open air. The overall yield was about 90%, and the purity was high based on Nuclear Magnetic Resonance and Fourier transform infrared analysis. ^{1}H NMR (500 MHz, $CDCl_3$, δ): 8.20 (d, 4H, Ar–*H*), 4.11 (t, 4H, N–CH_2), 3.83 (q, 12H, O–CH_2), 1.85 (m, 4H, N–CH_2CH_2), 1.24 (t, 18H, OCH_2CH_3), 0.75 (t, 4H, $SiCH_2$); ^{13}C NMR (500 MHz, DMSO, δ): 163.34 (*C*=O); 134.62, 131.11, 129.52, 126.41, 124.00, 123.91, 58.99 (OCH_2); 43.71 (N–*C*H_2) 22.43 (N–CH_2CH_2); 18.86 (OCH_2CH_3); 9.01 (Si–*C*H_2); FT-IR (KBr): ν = 3459, 2974, 2927, 1693, 1656, 1596, 1578, 1344, 1103, 1077, 811, 779, 746,485 cm^{-1}.

Synthesis of PDBS Assemblies: A specified volume of petroleum ether (boiling point 60–80 °C) or water was added to the pre-prepared PDBS/THF solution at room temperature. The volume ratio of THF to petroleum ether or water was maintained as 1/5. The mixtures were then coated on glass or mica substrates with substrate temperatures ranging from 25 to 90 °C. Subsequent solvent evaporation at controlled rates resulted in the formation of assemblies with tube, fiber, or spherical morphologies. Further hydrolysis and condensation of the triethoxysilane moieties within the resultant assemblies were conducted by exposing them to an acidic solution (pH = 1).

The chemical structures of the PDBS assemblies were examined using the FTIR (Thermo Nicolet Nexus^{TM} 670) and NMR (GE Omega PSG500 500 MHz). The crystal structure of PDBS molecules was determined by single crystal X-ray diffraction (Enraf-Nonius CAD-4 diffractometer). The morphology study was conducted by emission electron microscope (LEO 1550 VP at 10 kV), fluorescence and visible microscopy (on an Olympus IMT-2 inverted microscope connected to a high-resolution monitor (SONY) and an S-VHS VCR through an Optronics CCD camera). The observations by fluorescence microscopy were conducted at λ_{ex} = 490 nm. The nanocomposites were further characterized by transmission electron microscope (JEOL 2010 microscope operated at 120 kV) and powder X-ray diffraction (XRD) patterns (Siemens D500 diffractometer operating at 40 kV, 30 mA, Cu-Kα radiation, λ = 0.15406 nm). Thermal analysis was

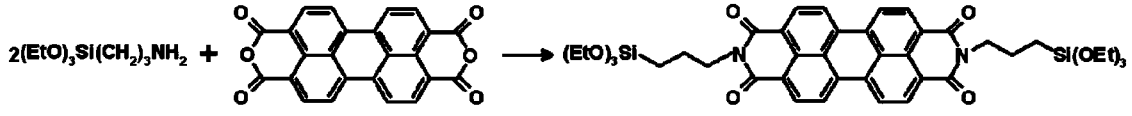

Scheme 1. Scheme of the synthesis of the PDBS building block.

conducted on a Thermogravimetric Analyzer (TGA) 2950 by TA instruments run at 15 °C min^{-1} from 25 to 1000 °C with argon sweep gas. The electronic properties were examined using UV-vis spectrophotometer (Beckman™ DU 640B Ultraviolet-visible). The conductivity of PDBS tubes and fibers was recorded over a frequency range of 10 to 1×10^7 Hz using a Solartron® 1260 gain phase analyzer.

Received: June 21, 2007
Revised: February 1, 2008
Published online: May 6, 2008

[1] B. Vigolo, A. Penicaud, C. Coulon, C. Sauder, R. Pailler, C. Journet, P. Bernier, P. Poulin, *Science* **2000**, *290*, 1331.
[2] a) L. Zhang, K. Yu, A. Eisenberg, *Science* **1996**, *272*, 1777. b) H. Peng, D. Chen, M. Jiang, *J. Phys. Chem. B* **2003**, *107*, 12462. c) H. Peng, D. Chen, M. Jiang, *Macromolecules* **2005**, *38*, 3550. d) D. Chen, H. Peng, M. Jiang, *Macromolecules* **2003**, *36*, 2576.
[3] a) J. M. Smeenk, P. Schon, M. B. J. Otten, S. Speller, H. G. Stunnenberg, J. C. M. van Hest, *Macromolecules* **2006**, *39*, 2989. b) D. E. Discher, A. Eisenberg, *Science* **2002**, *297*, 967. c) H. Peng, D. Chen, M. Jiang, *Langmuir* **2003**, *19*, 10989. d) I. O. Shklyarevskiy, P. Jonkheijm, P. C. M. Christianen, A. P. H. J. Schenning, E. W. Meijer, O. Henze, A. F. M. Kilbinger, W. J. Feast, A. D. Guerzo, J.-P. Desvergne, J. C. Maan, *J. Am. Chem. Soc.* **2005**, *127*, 1112.
[4] R. Oda, I. Huc, M. Schmutz, S. J. Candau, F. C. Mackintosh, *Nature* **1999**, *399*, 566.
[5] Y. Luo, J. Lin, H. Duan, J. Zhang, C. Lin, *Chem. Mater.* **2005**, *17*, 2234.
[6] H. Peng, Y. Lu, *Langmuir* **2006**, *22*, 5525.
[7] a) H. Engelkamp, S. Middelbeek, R. J. M. Nolte, *Science* **1999**, *284*, 785. b) M. Morikawa, M. Yoshihara, T. Endo, N. Kimizuka, *J. Am. Chem. Soc.* **2005**, *127*, 1358.
[8] a) W. Jin, T. Fukushima, A. Kosaka, M. Niki, N. Ishii, T. Aida, *J. Am. Chem. Soc.* **2005**, *127*, 8284. b) D. Yan, Y. Zhou, J. Hou, *Science* **2004**, *303*, 65. c) G. J. Jiang, L. Wang, T. Chen, H. Yu, C. Wang, C. Chen, *Polymer* **2005**, *46*, 5353.
[9] N. Zheng, X. Bu, P. Feng, *J. Am. Chem. Soc.* **2002**, *124*, 9688.
[10] a) S. M. Grayson, J. M. Frechet, *J. Chem. Rev.* **2001**, *101*, 3819. b) W.-D. Jang, D.-L. Jiang, T. Aida, *J. Am. Chem. Soc.* **2000**, *122*, 3232.
[11] a) L. Zhang, A. Eisenberg, *Science* **1995**, *268*, 1728. b) L. Zhang, K. Yu, A. Eisenberg, *Science* **1996**, *272*, 1777.
[12] L. Brunsveld, E. W. Meijer, R. B. Prince, J. S. Moore, *J. Am. Chem. Soc.* **2001**, *123*, 7978.
[13] a) H. Peng, J. Tang, J. Pang, D. Chen, L. Yang, H. S. Ashbaugh, C. J. Brinker, Z. Yang, Y. Lu, *J. Am. Chem. Soc.* **2005**, *127*, 12982. b) H. Peng, J. Tang, L. Yang, J. Pang, H. S. Ashbaugh, C. J. Brinker, Z. Yang, Y. Lu, *J. Am. Chem. Soc.* **2006**, *128*, 5304.
[14] a) K. D. Belfield, K. J. Schafer, M. D. Alexander, *Chem. Mater.* **2000**, *12*, 1184. b) A. Yakimov, S. R. Forrest, *Appl. Phys. Lett.* **2002**, *80*, 1667.
[15] K.-Y. Law, *Chem. Rev.* **1993**, *93*, 449.
[16] G. Seybold, G. Wangenblast, *Dyes Pigm.* **1989**, *11*, 303.
[17] a) C. W. Struijk, A. B. Sieval, J. E. J. Dakhorst, M. V. Dijk, P. Kimkes, R. B. M. Koehorst, H. Donker, T. J. Schaafsma, S. J. Picken, A. M. van de Craats, J. M. Warman, H. Zuilhof, E. J. R. Sudholter, *J. Am. Chem. Soc.* **2000**, *122*, 11057. b) C. D. Dimitrakopoulos, P. R. L. Malenfact, *Adv. Mater.* **2002**, *14*, 99.
[18] A. Xie, B. Liu, J. E. Hall, S. L. Barron, D. A. Higgins, *Langmuir* **2005**, *21*, 4149.
[19] a) F. Lu, Y. Yang, A. Sellinger, M. Lu, J. Huang, H. Fan, R. Haddad, G. Lopez, A. R. Burns, D. Y. Sasaki, J. Shelnutt, C. J. Brinker, *Nature* **2001**, *410*, 913. b) Y. Lu, H. Fan, N. Doke, D. A. Loy, R. A. Assink, D. A. LaVan, C. J. Brinker, *J. Am. Chem. Soc.* **2000**, *122*, 5258. c) Y. Yang, Y. Lu, M. C. Lu, J. M. Huang, R. Haddad, G. Xomeritakis, N. G. Liu, A. P. Malanoski, D. Sturmayr, H. Fan, D. Y. Sasaki, R. A. Assink, J. A. Shelnutt, F. V. Swol, G. P. Lopez, A. R. Burns, C. J. Brinker, *J. Am. Chem. Soc.* **2003**, *125*, 1269.
[20] N. G. Liu, K. Yu, B. Smarsly, D. R. Dunphy, Y.-B. Jiang, C. J. Brinker, *J. Am. Chem. Soc.* **2002**, *124*, 14540.
[21] a) J. J. E. Moreau, B. P. Pichon, M. Wong Chi Man, C. Bied, H. Pritzkow, J.-L. Bantignies, P. Dieudonne, J.-L. Sauvajol, *Angew. Chem. Int. Ed.* **2004**, *43*, 203. b) J. J. E. Moreau, L. Vellutini, M. Wong Chi Man, C. Bied, J.-L. Bantignies, P. Dieudonne, J.-L. Sauvajol, *J. Am. Chem. Soc.* **2001**, *123*, 7957.
[22] M. P. Kapoor, Q. H. Yang, S. J. Inagaki, *J. Am. Chem. Soc.* **2002**, *124*, 15176.
[23] R. J. P. Corriu, J. J. E. Moreau, P. Thepot, M. Wong Chi Man, *Chem. Mater.* **1992**, *4*, 1217.
[24] S. Inagaki, S. Guan, Y. Fukushima, T. Ohsuna, O. Terasaki, *J. Am. Chem. Soc.* **1999**, *121*, 9611.
[25] S. Guan, S. Inagaki, T. Ohsuna, O. Terasaki, *J. Am. Chem. Soc.* **2000**, *122*, 5660.
[26] B. J. Melde, B. T. Holland, C. F. Blanford, A. Stein, *Chem. Mater.* **1999**, *11*, 3302.
[27] A. Stein, B. J. Melde, R. C. Schroden, *Adv. Mater.* **2000**, *12*, 1403.
[28] T. Asefa, M. J. MacLachlan, N. Coombs, G. A. Ozin, *Nature* **1999**, *402*, 867.
[29] T. Asefa, M. J. MacLachlan, H. Grondey, N. Coombs, G. A. Ozin, *Angew. Chem. Int. Ed.* **2000**, *39*, 1808.
[30] Z. D. Popovic, R. O. Loutsy, A.-M. Hor, *Can. J. Chem.* **1985**, *63*, 134.
[31] B. A. Gregg, *J. Phys. Chem.* **1996**, *100*, 852.
[32] B. A. Gregg, J. Sprague, M. W. Peterson, *J. Phys. Chem. B* **1997**, *101*, 5362.
[33] R. A. Cormier, B. A. Gregg, *J. Phys. Chem. B* **1997**, *101*, 11004.
[34] R. A. Cormier, B. A. Gregg, *Chem. Mater.* **1998**, *10*, 1309.
[35] E. Lifshitz, A. Kaplan, E. Ehrenfreund, D. Meissner, *J. Phys. Chem. B* **1998**, *102*, 967.
[36] E. Lifshitz, A. Kaplan, E. Ehrenfreund, D. Meissner, *Chem. Phys. Lett.* **1999**, *300*, 626.
[37] S.-G. Liu, G. Sui, R. A. Cormier, R. M. Leblanc, B. A. Gregg, *J. Phys. Chem. B* **2002**, *106*, 1307.
[38] P. Yan, A. Chowdhury, W. M. Holman, D. M. Adams, *J. Phys. Chem. B* **2005**, *109*, 724.
[39] X. Zhang, Z. Chen, F. Würthner, *J. Am. Chem. Soc.* **2007**, *129*, 4886.
[40] M. Schneider, J. Hangen, D. Haarer, K. Müllen, *Adv. Mater.* **2000**, *12*, 351.
[41] T. Tang, J. Qu, K. Müllen, S. E. Webber, *Langmuir* **2006**, *22*, 26.
[42] B. A. Gregg, *J. Phys. Chem. B* **2003**, *107*, 4688.
[43] M. Mas-Torrent, M. Durkut, P. Hadley, X. Ribas, C. Rovira, *J. Am. Chem. Soc.* **2004**, *126*, 984.
[44] G. M. Whitesides, J. P. Mathias, C. T. Seto, *Science* **1991**, *254*, 1312.
[45] a) Z. Dai, L. Dahne, H. Möhwald, B. Tiersch, *Angew. Chem. Int. Ed.* **2002**, *41*, 4019. b) C. Gao, E. Donath, S. Moya, V. Dudnik, H. Möhwald, *Eur. Phys. J. E* **2001**, *5*, 21. c) S. Leporatti, C. Gao, A. Voigt, E. Donath, H. Möhwald, *Eur. Phys. J. E* **2001**, *5*, 13.
[46] P. Jonkheijm, N. Stutzmann, Z. Chen, D. M. de Leeuw, E. W. Meijer, A. P. H. J. Schenning, F. Wurthner, *J. Am. Chem. Soc.* **2006**, *128*, 9535.
[47] C. W. Struijk, A. B. Sieval, J. E. J. Dakhorst, M. van Dijk, P. Kimkes, R. B. M. Koehorst, H. Donker, T. J. Schaafsma, S. J. Picken, A. M. van de Craats, J. M. Warman, H. Zuilhof, E. J. R. Sudholter, *J. Am. Chem. Soc.* **2000**, *122*, 11057.
[48] D. A. Case, T. A. Darden, T. E. Cheatham, C. J. Simmerling, J. Wang, R. E. Duke, R. Luo, K. M. Merz, B. Wang, D. A. Pearlman, M. Crowley, S. Brozell, V. Tsui, H. Gohlke, J. Mongan, V. Hornak, G.

ADVANCED FUNCTIONAL MATERIALS

Cui, P. Beroza, C. Schafmeister, J. W. Caldwell, W. S. Ross, P. A. Kollman, AMBER 8, University of California, San Francisco **2004**.
[49] J. Wang, R. M. Wolf, J. W. Caldwell, P. A. Kollamn, D. A. Case, *J. Comput. Chem.* **2004**, *25*, 1157.
[50] T. A. Darden, D. York, L. Pedersen, *J. Chem. Phys.* **1993**, *98*, 10089.
[51] J. P. Ryckaert, G. Ciccotti, H. J. C. Berendsen, *J. Comput. Phys.* **1977**, *23*, 327.
[52] H. J. C. Berendsen, J. P. M. Postma, W. F. van Gunsteren, A. DiNola, J. R. Haak, *J. Chem. Phys.* **1984**, *81*, 3684.
[53] F. Wurthner, *Chem. Commun.* **2004**, 1564.